# Chapter 7
# Carbonation Mechanisms and Modelling

**Abstract** From the view point of reaction kinetics, many researchers have attributed the rate-determined step of aqueous carbonation to the reacted (product) layer diffusion. Therefore, this suggests that a well-designed reactor to enhance the mass transfer between the gas, liquid, and solid phases is needed to facilitate the carbonation reaction and increase the carbonation conversion. This chapter provides the principles and mechanisms of carbonation reaction using alkaline solid wastes. The kinetics of the major three steps of carbonation, i.e., metal ion leaching, $CO_2$ dissolution, and carbonate precipitation, are illustrated. Moreover, several classical heterogeneous kinetic models, e.g., shrinking core model and surface coverage model, are presented. Furthermore, the modeling of mass transfer for carbonation in various reactors and/or processes is summarized and discussed.

## 7.1 Carbonation Mechanisms

### *7.1.1 Principles*

As discussed in Chap. 5, the process chemistry of accelerated carbonation using alkaline solid wastes can be briefly divided into three steps:

- Step 1: Contemporary dissolution of $CO_2$ into a liquid phase and conversion of carbonic acid to carbonate/bicarbonate ions
- Step 2: Dissolution of $CO_2$-reactive species from a solid matrix (irreversible hydration)
- Step 3: Consequent nucleation and precipitation of carbonates

At first, the leaching of Ca-bearing compounds in alkaline solid waste would directly generate the $Ca^{2+}$ in the solution. Secondly, gaseous $CO_2$ can rapidly dissolve into the alkaline solution, where the predominant carbonate ions ($CO_3^{2-}$) could reduce the pH of the solution. Since the $CO_2$ continuously dissolved into the solution during the carbonation, the pH value would decrease gradually to 6.3,



P.-C. Chiang and S.-Y. Pan, *Carbon Dioxide Mineralization and Utilization*, DOI 10.1007/978-981-10-3268-4_7

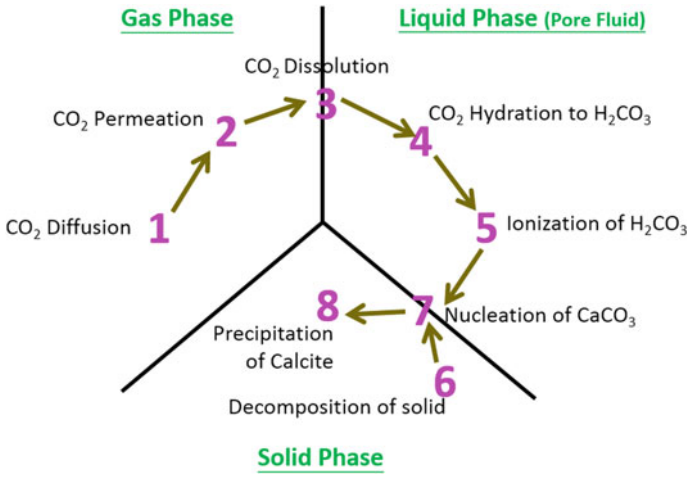


**Fig. 7.1** Schematic of accelerated carbonation mechanism

where the bicarbonate ions ($HCO_3^-$) were found to be dominated. Finally, $CaCO_3$ would be formed by reacting the calcium ions with the carbonate ions ($CO_3^{2-}$) and bicarbonate ions ($HCO_3^-$) in the solution under a high pH and circum-neutral condition, respectively. The above statements can be also divided into eight steps, as shown in Fig. 7.1.

It is widely accepted that the carbonation is controlled by the dissolution of $CO_2$, and therefore the reaction occurs on the liquid side near the interface between gas and liquid phases [1]. It suggests that the irreversible hydration of CaO proceeds spontaneously with carbonation of $Ca(OH)_2$ suspension [2, 3]. Moreover, not only $Ca(OH)_2$ but also other hydrate compounds, such as calcium–silicate–hydrates (C–S–H), can react with $CO_2$ to produce $CaCO_3$ and a silica gel [4]. The balance between dissolution and precipitation is dependent on the kinetics and solubility of the present feedstock and possible products, where carbonates are probably the most important products [5].

For $\gamma$–$C_2S$ phase (dominate component in steel slag), it does not react with water at normal temperature because the leaching of $Ca^{2+}$ and $O^{2-}$ (or $OH^-$) is very low [4]. Fernández-Bertos et al. [6] suggested that $CaCO_3$ can be directly formed in the carbonation of $\gamma$–$C_2S$ without the formation of intermediate products such as $Ca(OH)_2$, due to the catalytic action of capillary water. The breakdown of $C_2S$ and the formation of calcite can be observed by XRD, as indicated in Eq. (7.1):

$$\begin{aligned} 3CaO{\bullet}SiO_2 + y\,H_2O + (3\text{-}x)\,CO_2 &\rightarrow x\,CaO{\bullet}SiO_2{\bullet}yH_2O + (3\text{-}x)\,CaCO_3 \\ &\longrightarrow z\,CO_2 \rightarrow (x\text{-}z)\,CaO{\bullet}SiO_2{\bullet}yH_2O + z\,CaCO_3 \end{aligned} \tag{7.1}$$

### 7.1.2 Key Factors and Operating Parameters

For process design and system optimization, it is crucial to identify the effect of key operating factors on carbonation performance. Carbonation of alkaline solid wastes has been proved to be an effective way to capture $CO_2$. Several factors can affect the rate and extent of carbonation [7, 8]:

- Transportation-controlled mechanisms such as $CO_2$ and $Ca^{2+}$ ions diffusion to/from reaction sites
- Boundary layer effects (diffusion across precipitate coatings on particles)
- Dissolution of $Ca(OH)_2$ at the particle surface
- Pore blockage
- Precipitate coating

Table 7.1 summarizes the key factors required for effective accelerated carbonation. These operating factors must be clearly understood, since they determine the economic viability of the technology as well as help to identify the conditions that are the most favorable to the carbonation reaction.

#### 7.1.2.1 Particle Size and Surface Area

Both particle size and specific surface area are the most important factors affecting the dissolution kinetics of materials [9, 10]. It was noted that over 90% and less than 40% of calcium species can be dissolved in 24 h from 45–75 to 150–250-μm-sized ladle slag, respectively [11]. Since solid waste grinding is expected to be a fairly energy-intensive process, it is important to find out the optimal particle size for accelerated carbonation. For the steel slag, average particle sizes of less than 100–150 μm are suggested to be in the optimum range for

**Table 7.1** Key operating factors required for effective carbonation

| Phases | Physical properties | Chemical properties |
|---|---|---|
| Solid phase | • Particle size<br>• Mineralogy<br>• Specific surface area<br>• Porosity/Permeability<br>• Surface activities<br>• Microstructure | • Compositions (e.g., Ca and f-CaO content, Ca/Si ratio, Ferrite/$C_3A$ ratio)<br>• Heavy metals (e.g., Pb, Cd, Ni, Cr)<br>• Free water content<br>• Permeability |
| Liquid phase | • Temperature<br>• Liquid-to-solid ratio | • Organics/Inorganic<br>• Anions/Cations<br>• pH (or alkalinity)<br>• Permeability |
| Gas phase | • Partial pressure<br>• Flow rate<br>• Relative humidity<br>• Temperature | • $CO_2$ concentration<br>• Organics/Inorganic<br>• Particulate matter contents<br>• Other air pollutants (e.g., $SO_2$) |

efficient carbonation [12]. Similarly, Eloneva et al. [13] suggested that a particle size preferably of 100 μm, or no more than 500 μm, should be optimal, based on the kinetics studies of calcium leaching.

#### 7.1.2.2 Reaction Temperature

Reaction temperature is an important operating factor in the carbonation reaction. Temperature exhibits a significant effect on dissolution and carbonation performance, especially during the first 3 h of the dissolution reaction [11]. Each carbonation reaction mechanism exhibits a different sensitivity to the reaction temperature.

- Leaching of metal oxide from solid matrix: The dissolution kinetics of the calcium species could be enhanced by increasing the temperature.
- $CO_2$ dissolution into solution: The amounts of $CO_2$ dissolution into the solution decreased at higher temperature, which is detrimental to the carbonation reaction.
- Carbonate precipitate nucleation: The nucleation and growth of $CaCO_3$ are retarded at higher temperatures due to the decreased solubility of $CO_2$. On the other hand, the carbonation rate significantly increased with increasing reaction temperature.

Typically, a reaction temperature higher than 80 °C is unfavorable for the process design of direct carbonation [14], and 60 °C should be high enough for efficient dissolution and carbonation [15, 16].

#### 7.1.2.3 Liquid-to-Solid (L/S) Ratio

Liquid-to-solid (L/S) ratio determines the leaching capacity of Ca ion (and other ions) from the solid wastes to the solution. In general, an incomplete hydration of calcium-bearing compounds from solid wastes is always observed. For example, the measured leaching concentration of calcium was about 700−900 ppm, equivalent to a fraction of calcium leaching from the steel slag of 0.5−4.0% [17]. If the solubility of pure CaO (i.e., lime) at 20 °C was assumed to be 1.25 g/L [18], the theoretical concentration of calcium ions in water should be 892.9 mg/L. This indicates that the content of lime might be essentially controlling the solubility of CaO-related species in steel slag. In other words, the calcium leaching should be a solubility-controlled step, as a result of equilibrium with specified mineral phases, thereby resulting in an almost constant concentration in solution irrespective of the L/S ratio [17].

For municipal solid waste incineration fly ashes, Li et al. [19] found that the optimum L/S ratio for accelerated carbonation was 0.3 by weight of ash at ambient temperature. Similarly, the optimum L/S ratio was 0.2–0.3 for air pollution control

residues and 0.3–0.4 for bottom ash residues [20]. For iron and steel slags, Chang et al. [21, 22] suggested that the optimum L/S ratio for carbonation of steelmaking slag is 10–20 (mL $g^{-1}$).

#### 7.1.2.4 Solution Compositions ($CO_2$ Concentration and pH)

The performance of carbonation is highly related to the compositions of the solution. From the $CO_2$ concentration point of view, the reaction time should be inversely proportional to the $CO_2$ content of the ingoing gas flow; the lower the gas $CO_2$ content is, the longer the duration of the carbonation is. However, the $CO_2$ content of the incoming gas did not seem to have a significant effect on the degree of $CaCO_3$ precipitation.

The pH value of solution is another important factor related to the rate of calcium leaching, the rate of $CO_2$ dissolution, and the rate of $CaCO_3$ nucleation. The pH decreases continuously as carbonation proceeds due to $CO_2$ dissolution into solution. There is no change in pH after the carbonation is completed. On the other hand, it has been reported that sodium and potassium ions should cause pH fluctuations and also affect the carbonation rate [23]. It is noted that the dissolution of calcium components in solid wastes is favored at the low pH and high temperature, which is, however, not favored for the precipitation of $CaCO_3$. It also affects the specific species that can be precipitated during the carbonation [24, 25]. It suggests that the optimum pH for aqueous carbonation is around 10, while the dissolution of steel slag occurs under low pH conditions [26].

## 7.2 Reaction Kinetics

According to the mechanism of carbonation reaction as mentioned before, the overall reaction kinetics for the accelerated carbonation can be divided into three parts: (1) metal ion leaching from solid matrix; (2) $CO_2$ dissolution into solution; and (3) carbonate precipitation. Several theoretical kinetic models regarding the above three parts are illustrated as follows.

### *7.2.1 Metal Ion Leaching from Solid Matrix*

The release of metal ions to the water solution, so-called leaching, depends on their solution speciation and their affinity to bind to reactive surface in the solid matrix and pore water. To evaluate the leaching performance of a certain process, "mass conservation model" could provide valuable insights into the speciation of metal ions in the solution phase. Moreover, evaluation of the pH dependence of leaching for various metal ions is a good approach to assessing the solid wastes, both for

research purposes as well as in the context of the development of regulation and standard operation procedure for leaching tests [27].

#### 7.2.1.1 Mass Conservation Model

The leaching concentrations of various metal ions are generally observed to increase rapidly in the beginning, and then gradually approach a maximum concentration. Therefore, the leaching kinetics of various metal ions ($i$) from the solid matrix can be evaluated by the mass loss-based method, as shown in Eq. (7.2):

$$r_i = \frac{\mathrm{d}C_i}{\mathrm{d}t} = k_i[C_{\max,i} - C_i]^{n_i} \tag{7.2}$$

where $r_i$ is the leaching rate of various metal ions, $k_i$ is the rate constant of leaching, $C_{\max,i}$ (mg/L) is the maximum leaching concentration for various metal ions in solution, $C_i$ (mg/L) is the leaching concentration of various metal ions, where the background concentration of metal ions originally in the solution was subtracted, and $n_i$ is the order of leaching reaction of various metal ions. Equation (7.3) can be integrated as follows:

$$C_i = C_{\max,i}\left[1 - \mathrm{e}^{-k_i t}\right], \quad \text{for } n = 1 \tag{7.3a}$$

$$C_i = C_{\max,i} - [C_{\max,i}^{1-n} - (1-n)k_i t]^{1/(1-n)}, \quad \text{for } n \neq 1 \tag{7.3b}$$

In general, both the values of $C_{\max}$ and $k$ are observed to increase as the particle size of solid waste decreased. In the case of steel slag, the leaching behavior of Ca, Na, K, and Fe ions was found to be more sensitive to the concentration driving force than that of others because the obtained $n$ values were greater than one.

#### 7.2.1.2 Leaching Kinetics for Alkaline Solid Wastes

Calcium (Ca), sodium (Na), and potassium (K) metal ions are found to be the major ions leaching out from in the case of steel slag [10]. Steel slag normally contained a great amount of reactive Ca-bearing phases including lime (CaO), portlandite ($Ca(OH)_2$), and larnite ($Ca_2SiO_4$). This might account for most of the calcium leaching concentration from the steel slag.

On the other hand, both Pb and Zn are considered minor elements that might not affect the carbonation reaction. Similarly, Fe, Al, and Mg are considered slightly released cations because the measured concentrations in the solution typically remain low over the leaching time ($\sim$90 min). It might be attributed to the low mobility of Mg–Fe–Al–Si oxides, where Mg and Al are commonly associated with Fe-bearing phases in steel slag. In most curriculums, Mg release was found to be

quite low compared to Ca release, which implies that the formation of $MgCO_3$ should be negligible [10, 16].

Also, the releases of Ni and Cr ions are quite low, and the concentration of Ni and Cr remained almost constant. For example, in the case of steel slag, the concentration of Ni and Cr was approximately 7.1–10.4 and 2.0–3.3 mg/L, respectively, during the entire leaching time of 90 min [10]. According to De Windt et al. [28], the maximum Cr leaching concentration in deionized (DI) water was about 0.015 ppm at a liquid-to-solid (L/S) ratio of 10.

#### 7.2.1.3 Factors Affecting Leaching Kinetics

The rate and extent of calcium leaching are inversely related to particle size and pH, and increased with increasing temperature, pressure, and surface area [28, 29]. The effects of increased reaction temperature from 25 to 50 °C provided a 70% improvement on the dissolution of the primary phase [30]. However, a higher reaction temperature would reduce the dissolution of $CO_2$ in water, which is disadvantageous to calcite precipitation [21, 31].

Other factors may hinder the leaching of metal ions, thereby leading to a lowering of mass-transfer rate:

- Lack of porosity in solid wastes
- Formation of protective layer on the surface of particles
- Over saturation of metal ions in the solution
- Insufficient stirring and mixing between solid and liquid phases
- Severe agglomeration of (fine) particles in the solution

The leaching of $Ca^{2+}$ ions should result in a withdrawing Ca–silicate core surrounded by a Ca-depleted $SiO_2$ phase [32, 33]. This $SiO_2$ rim apparently hindered the diffusion of $Ca^{2+}$ ions from the interior of the particle, resulting in a declining reaction rate. Hence, $Ca^{2+}$ ions' leaching rate, probably determined by diffusion through the Ca-depleted silicate rim, rather than by the boundary layer at the solid–liquid interface, seems to be the main rate-limiting step in aqueous carbonation.

### 7.2.2 *$CO_2$ Dissolution into Solution*

The kinetics of dissolution of $CO_2$ and dehydration of $H_2CO_3$ has been studied intensively [23, 34]. These two reactions should occur simultaneously, as shown in Eq. (7.4):

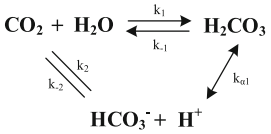


(7.4)

The rate expression of the dissolution–dehydration reaction is:

$$-\frac{\mathrm{d}[\mathrm{CO_2}]}{\mathrm{d}t} = (k_1 + k_2)[\mathrm{CO_2}] - k_{-1}[\mathrm{H_2CO_3}] - k_{-2}\left[\mathrm{HCO_3^-}\right][\mathrm{H^+}] \tag{7.5}$$

By substituting Eq. (7.4) into Eq. (7.5), we obtain

$$\begin{aligned} -\frac{\mathrm{d}[\mathrm{CO_2}]}{\mathrm{d}t} &= (k_1 + k_2)[\mathrm{CO_2}] - (k_{-1} + k_{-2}K_{\alpha 1})[\mathrm{H_2CO_3}] \\ &= k_{\mathrm{CO_2}}[\mathrm{CO_2}] - k_{\mathrm{H_2CO_3}}[\mathrm{H_2CO_3}] \end{aligned} \tag{7.6}$$

where the overall rate constants in Eq. (7.5) were simplified to be $k_{\mathrm{CO_2}}$ and $k_{\mathrm{H_2CO_3}}$. The values of $k_{\mathrm{CO_2}}$ and $k_{\mathrm{H_2CO_3}}$ at 25 °C were 0.032 and 26.6 $\mathrm{s^{-1}}$, respectively [35]. However, at higher pH (e.g., pH higher than 9), an alternative reaction pathway would be expressed as

$$\mathrm{CO_2} + \mathrm{OH^-} \overset{k_4}{\leftrightarrow} \mathrm{HCO_3^-} \tag{7.7}$$

where $k_4$ (i.e., 8500 $\mathrm{M^{-1}\ s^{-1}}$ at 25 °C) and $k_{-4}$ (i.e., 0.0002 $\mathrm{s^{-1}}$ at 25 °C) are the rate constants [36].

### *7.2.3 Carbonate Precipitation*

Carbonation reaction is regulated by solution equilibrium, and the reaction of calcium ions combining with carbonate ions is very fast. Several models, such as simplified first-order model, saturation state model, and heterogeneous dissolution–precipitation model, have been extensively applied for determining the kinetic parameters of carbonation reaction.

#### 7.2.3.1 Simplified First-Order Model

It is suggested that the accelerated carbonation is a first-order reaction, with respect to the concentrations of $\mathrm{Ca^{2+}}$ and $\mathrm{CO_3}^{2-}$ [23]. In other words, the precipitation rate is related to the $\mathrm{CO_3^{2-}}$ concentration in the liquid phase, but not to the concentration of other species containing carbonate. Therefore, the rate of carbonation can be described by the following Eq. (7.8):

$$Q_{\mathrm{CO_2}} = \frac{\mathrm{d}(C_{\mathrm{CaCO_3}})}{\mathrm{d}t} = -\frac{\mathrm{d}(\mathrm{CO_3^{2-}})}{\mathrm{d}t} = k\left[\mathrm{Ca^{2+}}\right]\left[\mathrm{CO_3^{2-}}\right] \tag{7.8}$$

where $C_{CaCO_3}$ is the concentration of calcium carbonate (mole $L^{-1}$), and $k$ is the reaction rate constant ($mol^{-1}$ $s^{-1}$). The rate constant ($k$) is dependent on the reaction temperature according to Arrhenius's law. The Boltzmann distribution law can also be applied to determine the ratio of the molecule having a kinetic energy above the activation energy of the chemical reaction. The $k$ value reported by Ishida and Maekawa [23] was 2.08 (L $mol^{-1}$ $s^{-1}$) at 25 °C from several sensitivity analyses.

#### 7.2.3.2 Saturation State Model

The kinetic rate laws for weathering of rock-forming minerals can be in principle applied to the leaching of solid wastes, since these materials consist of well-crystallized solid phases. A simple kinetic formulation without any pH dependency can be used for the dissolution of a primary mineral phase ($M_i$) [28]:

$$r_i = \frac{d[M_i]}{dt} = k_i A_i \left( \frac{Q_i}{K_i^{-1}} - 1 \right) \tag{7.9}$$

where the $k_i$ is the intrinsic rate constant far from equilibrium; $A_i$ is the mineral surface area; $Q_i$ stands for the ion activity product; and $K_i$ is the thermodynamic formation constant. It is noted that the term $(Q_i/K_i^{-1} - 1)$ is the saturation state. At equilibrium, this term becomes zero, and likewise so does the kinetic rate [28].

#### 7.2.3.3 Heterogeneous Dissolution–Precipitation Model

Reaction with $CO_2$ will lower the pH of slurry; therefore, the minerals will keep dissolving in the course of the carbonation. In other words, as the calcium ions are converted to $CaCO_3$ precipitates, more calcium hydroxide dissolves to equalize the concentration of metal ions. This reveals that precipitation kinetics is not equal to dissolution kinetics. Assuming the heterogeneous dissolution–precipitation reactions occur at the surface of a carbonate, the governing equation of carbonation rate can be expressed as follows [37]:

$$\text{rate} = k_0 \times A_s \times \exp\left( -\frac{E_a}{RT} \right) \times a_{H^+}^{n_H} \times \prod_i a_i^{n_i} \times g(I) \times f(A) \tag{7.10}$$

where $k_0$ is the rate constant; $A_s$ is the reactive surface are of the mineral; $E_a$ is the activate energy; $T$ is the activation energy (K); the term $a_{H+}^{nH}$ is the pH dependence of the rate of the dissolution–precipitation reaction; the term $\prod_i a_i^{n_i}$ comprises possible catalytic or inhibitory effects linked to other solution; and the terms $g(I)$ and $f(A)$ account for the dependence of the rate on the ionic strength $I$ of the solution, and the ionic strength $I$ of the aqueous solution, respectively. The $\alpha$ is the fractional conversion, which can be expressed by

$$\frac{d\alpha}{dt} = A \times \exp\left(-\frac{E_A}{RT}\right) \times f(\alpha) \tag{7.11}$$

$$g(\alpha) = \int \frac{d\alpha}{f(\alpha)} = \int A \times \exp\left(-\frac{E_A}{RT}\right) dt \tag{7.12}$$

$$f(\alpha) = \frac{-1}{\ln(1-\alpha)} \tag{7.13}$$

Although the $Ca^{2+}$ ion dissolution kinetics can be improved with the increase in temperature, carbonation precipitation is retarded at higher temperatures due to reduced $CO_2$ solubility [31, 38]. In some circumstance using steel slag under ambient conditions, limited $MgCO_3$ formation from carbonation is expected due to the relatively low magnesium oxide content in the slag, low pressure of $CO_2$, and short reaction times. Via aqueous carbonation, typical process conditions for the formation of magnesium carbonation are a pressure of $CO_2$ ($p_{CO_2}$) higher than 100 bar for hours [39]. However, $MgCO_3$ formation can be observed when natural ores (e.g., serpentine and olivine) are used for carbonation [40, 41], as discussed in Chap. 10.

## 7.3 Classical Heterogeneous Kinetic Models

Several classical (theoretical) models, such as random pore model [42], overlapping grain model [43], shrinking core model [11, 16], and surface coverage model [44], are available for simulating the performance of accelerated carbonation using a CaO-based material. For the sake of simplicity, different assumptions should be made by each model to avoid complicated calculations.

### *7.3.1 Shrinking Core Model*

Shrinking core model (SCM), developed by Sohn and Szekely [45], has been applied for kinetic analysis of heterogeneous reactions, such as the carbonation reactions of solid particles [11, 22], because of its conceptual and mathematical simplicity. A primary assumption under the SCM is that the reaction occurs first at the outer layer of the particle and then proceeds into the inside of the particle, leaving behind the completely reacted product and the reactive-species-depleted rims referred to as the “ash” and/or “product” layer [11, 22, 46]. Therefore, at any time, an unreacted core of material exists, which shrinks in size during the reaction.

#### 7.3.1.1 Classic Governing Equations

Experimental data can be utilized to determine the kinetics and rate-determining step of a reaction based on the SCM. In the SCM, the governing equations of possible rate-determining steps, as shown in Fig. 7.2, include the following:

- Chemical reaction at the unreacted core surface (C-mechanism)
- Ash-layer diffusion (A-mechanism)
- Fluid-film diffusion (F-mechanism)

Let us consider a fluid–solid reaction of the following general expression:

$$CO_{2(\text{fluid})} + bCaO_{(\text{solid})} \rightarrow CaCO_{3(\text{s})} \tag{7.14}$$

where $b$ (–) is stoichiometric coefficient of a fluid–solid reaction, which can be assigned a value of one for carbonation reaction.

The overall radius of the solid particle ($R$) is assumed to remain constant, which is a primary assumption of SCM. Therefore, the time required for complete conversion of particle to product (i.e., carbonation conversion $\delta_{CaO} = 100\%$) for the mechanisms of chemical reaction, ash-layer diffusion, and film diffusion (i.e., $\tau_C$, $\tau_{A,}$ and $\tau_F$, respectively) can be obtained via various governing equation, as follows:

1. Chemical reaction at the un-reacted core surface (C-mechanism)

When the chemical reaction between reactants is the rate-limiting step, Eq. (7.15) shows the relationship between the carbonation conversion of alkaline solid waste ($\delta_{CaO}$) and reaction time ($t$, sec):

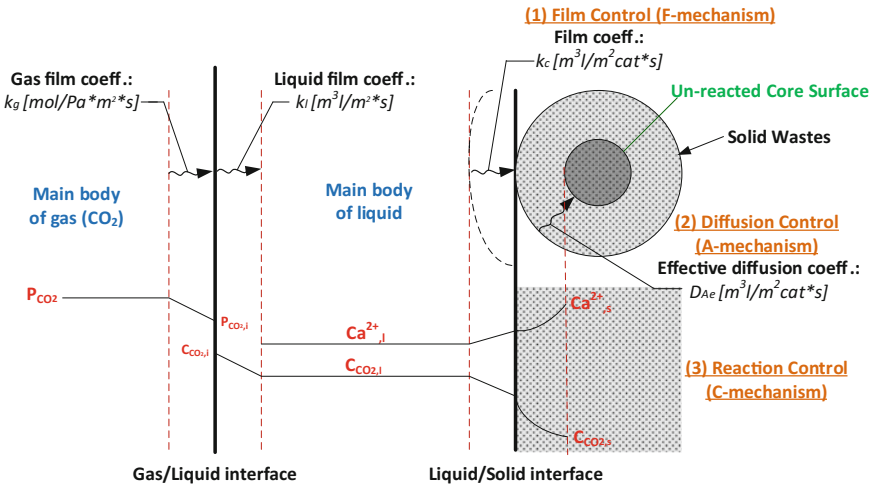


**Fig. 7.2** Diagram of phase transition among gas, liquid, and solid phases for shrinking core model

$$t = \tau_C \times \left[1 - (1 - \delta_{CaO})^{1/3}\right] \tag{7.15}$$

where $\tau$ (s) is the time for complete conversion of a reactant particle to product.

For the C-mechanism, the relationship of $\tau_C$ and the rate constant for the surface reaction ($k''$, $s^{-1}$) is shown as Eq. (7.16):

$$\tau_C = \frac{\rho_B R}{b k'' C_{Ag}} \tag{7.16}$$

where $k''$ is the first-order rate constant for the surface reaction, the term $R$ (cm) is the radius of the particles, $\rho_B$ (mol $cm^{-3}$) is the molar density of particle, $C_{Ag}$ (mol $cm^{-3}$) is the concentration of $CO_2$ in the solution.

2. Ash-layer diffusion (A-mechanism)

When the diffusion of carbonate ions (i.e., reactant) through the ash layer is the rate-limiting step, the relationship between the carbonation conversion and reaction time can be illustrated by Eq. (7.17):

$$t = \tau_A \times \left[1 - 3(1 - \delta_{CaO})^{2/3} + 2(1 - \delta_{CaO})\right] \tag{7.17}$$

For the A-mechanism, the relationship of $\tau_A$ and the effective diffusivity of the reactant through the ash layer ($D_e$, $cm^2$ $s^{-1}$) is shown as Eq. (7.18):

$$\tau_A = \frac{\rho_B R^2}{6 b D_e C_{Ag}} \tag{7.18}$$

3. Fluid-film diffusion (F-mechanism)

When the mass transfer of the reactants through the boundary layer at the liquid–solid interface is the rate-limiting step, Eq. (7.19) shows the relationship between the conversion and reaction time:

$$t = \tau_F \times \delta_{CaO} \tag{7.19}$$

For the F-mechanism, the relationship of $\tau_F$ and the mass transfer coefficient ($k_e$, mol $m^{-2}$ $Pa^{-1}$ $s^{-1}$) is shown as Eq. (7.20):

$$\tau_F = \frac{\rho_B R}{3 b k_e C_{Ag}} \tag{7.20}$$

#### 7.3.1.2 Modified SCM for Considering Particle Size Changes with Reaction

Due to its conceptual and mathematical simplicity, classical SCM has been used to determine the rate-limiting step in a heterogeneous reaction. However, in the SCM, there is an inherent assumption that complete carbonation conversion of solid particle should be eventually reached. From the experimental data in the literature, the full carbonation conversion of particles will never occur, regardless of time allowed. This implies that other factors, such as mineralogy of particles, particle size changes, and pore blockage, should be considered in addition to the diffusion limit of reactants into the particles [17]. The mineralogical compositions of particles are complex [12], where some of mineral phases do not react during carbonation. In actuality, the thickness of the ash layer would change with the reaction, which might affect the diffusivity of the gaseous reactant in the ash layer. To include the effect of particle size distribution on classical SCM, both "$Z$ factor" and a "$\lambda$ factor" [47] could be introduced to describe the relationship between the modified particle conversion ($\delta_{\mathrm{CaO}}$) and reaction time ($t$).

1. $Z$ factor

Sohn (2004) [48] included a $Z$ factor and modified the governing equation for pore diffusion control in SCM, as shown in Eq. (7.21), in the case where the volume of the solid product is different from that of the solid reactant, i.e., $R$ changes with conversion:

$$t = \tau_{\mathrm{A}} \times \left[ \frac{Z - (Z - (Z-1)(1-\delta_{\mathrm{CaO}}))^{2/3}}{(Z-1)/3} - 3(1-\delta_{\mathrm{CaO}})^{2/3} \right] \tag{7.21}$$

where $Z$ is the volume of product solid formed from a unit volume of reactant solid (both volumes include those of pores), and the term $r$ is the particle size. If $Z$ is assigned a value of one (i.e., the overall volume of the solid product is the same as that of the solid reactant), Eq. (7.21) can be simplified to Eq. (7.17) for $Z = 1$ by applying L′ Hospital's rule.

2. $\lambda$ factor

A "$\lambda$ factor" [47] can be introduced to modify the carbonation conversion of solid particle with the changes in particle size with reaction, as shown in Eq. (7.22):

$$\delta_{\mathrm{CaO}} = 1 - \int_{\left(\frac{t}{-\lambda}\right)^{\frac{1}{\eta-D}}}^{r_{0,\max}} \frac{\left(\frac{t}{\lambda} + r^{\eta-D}\right)^{\frac{\eta}{\eta-D}}}{r^{\eta}} f(r)\mathrm{d}r \tag{7.22}$$

where $D$ is the fractal dimension of the particle external surface (i.e., $D \in [2, 3]$), and $\eta$ is a function of fractal dimension.

If the particle size remained unchanged in the course of reaction, then these modified models should be identical to the traditional SCM. Based on the SEM images, the size of precipitated calcium carbonate on the surface of the steel slag was found to range from 1 to 3 μm, which was significantly smaller than the steel slag [16]. In addition, in reality, the diffusion coefficient of $CO_2$ in the solution should be time-dependent, since the diffusion rate is a function of concentration gradient. The buffering capacity of the slurry will change with the different L/S ratios and reaction times, thereby resulting in different reactant concentrations ($C_{Ag}$) in solution because the $C_{Ag}$ also changes as a function of pH [17].

#### 7.3.1.3 Mechanisms and Diffusivity

To scale up and optimize the process, the key parameters for reactor design, such as mass-transfer coefficient and diffusivity of the reactant, can be obtained by the SCM. Information on the kinetic model of carbonation for determining the fluid-film diffusion-controlled and chemical-reaction-controlled conversions is provided in the previous sections. Lekakh et al. [11] evaluated the calcium leaching data of steelmaking slag to determine the rate-limiting step based on shrinking core model and found that during the initial stage (to 30% conversion), the rate-limiting step was chemical reaction controlled, and the later stage was controlled by diffusion. Similar observations were also found in other research that the dissolution step was generally assumed to be the rate-limiting step with respect to the overall carbonation reaction [32, 49].

Compared to the natural weathering process, aqueous carbonation is a rapid reaction because of rapid leaching of calcium ions from the particle surface of solid wastes [12]. For steel slag, it is suggested that the carbonation in a slurry reactor should be controlled by ash diffusion, which is verified through the SEM images of the steelmaking slag surface structure taken during the carbonation [6, 17]. The carbonation reaction would lead the reacted solid with a lower porosity, tortuosity, and pore area due to the formation of calcite. Since the reaction product $CaCO_3$ coated the particle surface, the pores of carbonated particles were blocked by the products. In addition, the calcite precipitate was formed as a protective layer around the reacting particles. Therefore, the diffusion paths were also blocked, resulting in a dynamic equilibrium. This indicates the rationale for applying the SCM for carbonation of alkaline solid wastes.

The carbonation reaction of alkaline solid wastes should be ash-diffusion controlled. The diffusivity ($D_e$) of reactant is also quite different among the feedstock, types of reactors, and operating conditions. For instance,

- Steelmaking slag with deionized water in a slurry reactor: from $2.88 \times 10^{-7}$ to $7.28 \times 10^{-7}$ $cm^2\ s^{-1}$ [22].
- Steelmaking slag with deionized water in high-gravity carbonation: from $5.47 \times 10^{-7}$ to $1.49 \times 10^{-6}$ $cm^2\ s^{-1}$ [16].

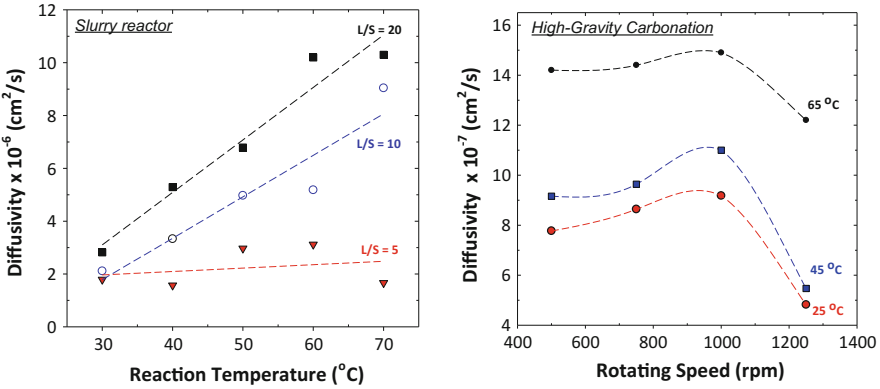


**Fig. 7.3** Variation in effective diffusivity with (*left*) reaction temperature in a slurry reactor ($P_{CO_2}$ = 1 bar; $CO_2$ flow rate = 0.1 L min$^{-1}$) and (*right*) rotating speed in high-gravity carbonation ($P_{CO_2}$ = 1 bar; slurry flow rate = 1.2 L min$^{-1}$; $D_p \sim 62$ μm; L/S = 20 mL g$^{-1}$)

- Steelmaking slag with deionized water in a slurry reactor: from $2.33 \times 10^{-8}$ to $4.67 \times 10^{-7}$ cm$^2$ s$^{-1}$ at temperatures of 30−70 °C [17].
- Bottom ash with cold-rolling wastewater in a slurry reactor: from $1.00 \times 10^{-6}$ to $2.90 \times 10^{-5}$ cm$^2$ s$^{-1}$ [50].

It was noted that the effective diffusivities measured in a slurry reactor and in a rotating packed bed exhibited the same magnitude of $10^{-6}$ cm$^2$ s$^{-1}$ [16]. Several examples for the effect of various operating factors on diffusivity are provided, as shown in Fig. 7.3. The $D_e$ value increases as the reaction temperature increases.

### 7.3.2 *Surface Coverage Model*

The surface coverage model was originally developed by considering the carbonation and desulfurization of hydrated lime at low temperatures by Shih et al. [51]. Their previous studies demonstrated that the surface coverage model was the most suitable model to describe the reaction between $Ca(OH)_2$ and $SO_2$ or $CO_2$. Those reaction behaviors are similar to the carbonation of steelmaking slag. Therefore, a surface coverage model could be utilized to determine the kinetics of the carbonation reaction. Figure 7.4 illustrates the mechanism of accelerated carbonation reaction of alkaline solid wastes, expressed by the surface coverage model.

It is noted that the kinetics of the carbonation reaction of alkaline solid wastes and the reaction rate constant could be described and estimated, respectively, by the surface coverage model [21, 44, 46]. The inherent assumptions of the surface coverage model include the following:

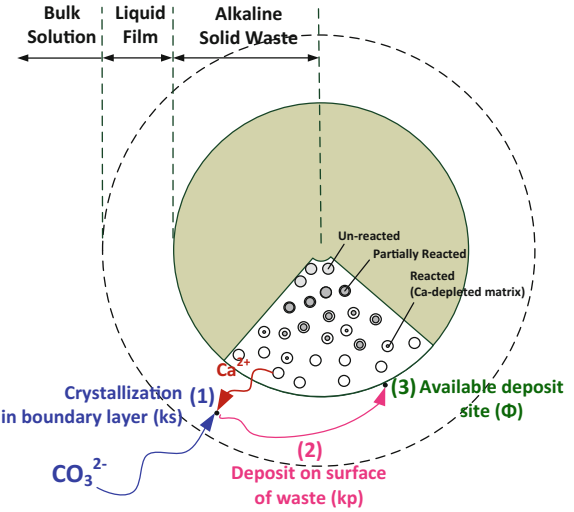


**Fig. 7.4** Conceptual diagram of assumptions of surface coverage model for accelerated carbonation reaction using alkaline solid wastes

- Reaction occurs only at un-reacted surface sites without being covered by the reaction product.
- The reaction product is deposited on the surface of the solid reactant.
- The fraction of the active surface sites ($\varphi$) that is still not covered by the reaction product changes with reaction times depending on the reaction rate.
- The solid reactant will reach a maximum conversion of reaction ($\delta_{max}$).

In the surface coverage model, the rate of carbonation conversion ($\delta_{CaO}$) can be expressed by Eq. (7.23) [20, 22]:

$$\frac{d\delta_{CaO}}{dt} = S_g M \cdot r_s = S_g M \cdot k_s \Phi \tag{7.23}$$

where $S_g$ ($m^2/g$) is the initial specific surface area of alkaline solid wastes; $M$ (g/mole) is the weight of alkaline solid wastes per mole of the reactive species (i.e., CaO); $r_s$ (mole/min/$m^2$) is the carbonation reaction rate per initial surface area of alkaline solid wastes; and $k_s$ (mole/min/$m^2$) is the overall rate constant. The fraction of the active surface sites ($\Phi$) that changes with reaction times can be expressed by Eq. (7.24):

$$-\frac{d\Phi}{dt} = k_p \Phi^{n-1} \cdot r_s = k_p \cdot k_s \Phi^n \tag{7.24}$$

where $k_p$ ($m^2$/mole) is a proportional constant reflecting the fraction of the active surface that is not covered by the reaction product. The principles and operating details of thermal analysis can be found in Chap. 6. Since calcium-bearing phases were assumed to be the major components participating in the carbonation reaction, the carbonation conversion ($\delta_{CaO}$) of alkaline solid wastes was calculated with a

TGA by measuring the weight loss caused by the thermal decomposition of $CaCO_3$ in alkaline solid wastes.

Moreover, the above kinetic rate constants can be simplified by assuming $k_1$ ($min^{-1}$) and $k_2$ (dimensionless), as shown in Eqs. (7.25) and (7.26), respectively:

$$k_1 = k_s S_g M \tag{7.25}$$

$$k_2 = k_p/(S_g M) \tag{7.26}$$

For the carbonation of hydrated lime, the standard deviations for $n$ = 1.0, 1.7, and 2.0 were found to be 0.015, 0.012, and 0.013, respectively, where $n$ = 1.7 is the best fitting value [24]. Since these standard deviation values were within the range of experimental error [24], it was difficult to determine the most appropriate rate expression ($n$ value). Consequently, it suggests that the $n$ value in Eq. (7.24) could be assigned to be one for simplicity. In other words, the integration of Eq. (7.23) can be used to describe the relationship between the carbonation conversion and reaction time, in terms of $k_1$ and $k_2$, by Eq. (7.27):

$$\delta_{CaO} = [1 - \exp(-k_1 k_2 t)]/k_2, \quad \text{for } n = 1 \tag{7.27}$$

The two terms, $k_1$ and $k_2$, in Eq. (7.27) can be obtained accordingly by least squares fitting to the experimental data of carbonation conversion and reaction time. Based on the surface coverage model, it is noted that the carbonation conversion of alkaline solid wastes would reach a maximum value under a specific condition. If the reaction time extends to the saturation time, the exponential term (i.e., exp $(-k_1 k_2 t)$) in Eq. (7.27) would approach to zero. The carbonation conversion of alkaline solid wastes can be then expressed as a constant value of the reciprocal of $k_2$. Therefore, Eq. (7.27) can be expressed, in terms of maximum carbonation conversion for alkaline solid wastes ($\delta_{max}$), as Eq. (7.28):

$$\delta_{CaO} = \delta_{max}\left[1 - \exp\left(-k_S k_p t\right)\right] \tag{7.28}$$

It is noted that the overall rate constant ($k_s$) is related to the following factors:

- The rate of gaseous $CO_2$ dissolution into solution
- The rate of calcium ions leaching from the solid matrix into solution,
- The rate of calcium carbonate precipitation

The $CaCO_3$ product deposited on the surface of reactant particle would hinder further leaching of the calcium species in the solid matrix into the solution. A higher $k_s$ might result in a greater amount of product formation on the surface of alkaline solid wastes at the beginning of the reaction, which would decrease the dissolution rate of unreacted calcium species from the inside alkaline solid wastes into solution afterward [44].

On the other hand, the active surface site of alkaline solid wastes would be gradually covered by the carbonated product during the reaction. Once the product

layer formed around the surface of alkaline solid wastes, the diffusion of reactants through the product layer would be the rate-limiting step for carbonation, hindering the alkaline solid wastes from further carbonation, thereby reaching a maximum carbonation conversion. In the course of carbonation, the surface structure of reacted alkaline solid wastes was found to change, where the small $CaCO_3$ particles were formed on the surface of alkaline solid wastes. Therefore, the carbonation reaction of alkaline solid wastes took place at the surface of alkaline solid wastes and formed a protective layer around the reacting particles. The rate of product deposition on the surface of the alkaline solid wastes ($k_s \cdot k_p$) was found to be higher at lower temperature [44]. This implies that carbonation would reach steady state much faster at lower temperatures than at higher temperatures. The leaching of calcium ions from alkaline solid wastes into solution can be accelerated as the reaction temperature increased. However, at higher temperatures, the precipitation of calcium carbonate was retarded due to the decrease in $CO_2$ solubility.

Table 7.2 compares the kinetic parameters of carbonation reaction for iron and steel slags via different processes, including high-gravity carbonation, slurry reactor, and autoclave reactor, by the surface coverage model.

The carbonation reaction rate per initial surface area ($k_S$) in different reactors is summarized as follows:

- Autoclave reactor: 0.8–2.6 mmol/min/$m^2$
- Slurry reactor: 0.3–0.5 mmol/min/$m^2$
- High-gravity carbonation process: 0.2–0.3 mmol/min/$m^2$

This might be attributed to the higher operating pressure of $CO_2$ (1400 psig) and reaction temperature (160 °C) performed in the autoclave reactor. However, operations with high pressure and temperature maintained in an autoclave reactor over a long period will require more energy and generate extra $CO_2$ emissions, which is not beneficial to the $CO_2$ capture process. In addition, in the slurry reactor, carbonation with alkaline wastewater (i.e., CRW) exhibited higher $k_s$ values (i.e., 0.7 mmol/min/$m^2$) than that using effluent water (i.e., 0.3 mmol/min/$m^2$) and DI water (i.e., 0.5 mmol/min/$m^2$). It is evident that the carbonation conversion in the wastewater/solid residues system could be higher than that in the pure water/solid residues system [34, 35]. On the other hand, regardless the initial surface area of particles, the overall rate constant ($k_1$) for DW in different reactors is summarized as follows:

- High-gravity carbonation process: 0.299 $min^{-1}$
- Slurry reactor: 0.227 $min^{-1}$
- Autoclave reactor: 0.033 $min^{-1}$

It was noted that carbonation of steel slag in the high-gravity carbonation process exhibits superior performance for $CO_2$ capture due to the highest carbonation conversion of solid waste with the greatest reaction kinetics and a lower reaction time. Generally, the carbonation conversion ($\delta_{CaO}$) of steel slag in the high-gravity carbonation process was found to be greater than that in the other two cases, i.e., the

**Table 7.2** Comparison of kinetic parameters for accelerated carbonation of steel slags via various types of processes

| Items | | Units | Results (surface coverage model) | | | | | | | |
|---|---|---|---|---|---|---|---|---|---|---|
| Reactor type | | – | Autoclave reactor[a] [21] | | | Slurry reactor[b] [46] | | | High-gravity carbonation [44] | |
| Liquid agents | | – | DW | DW | DW | DW | EW | CRW | DW | DW |
| Solid residues | | – | BHC | FAS | UFS | BOFS | BOFS | BOFS | BOFS | BOFS |
| Experiment | $\delta_{CaO}$ | – | 0.68 | 0.35 | 0.38 | 0.80 | 0.78 | 0.89 | 0.94[c] | 0.92[d] |
| Model parameters | $M$ | g/mole | 106.0 | 144.3 | 132.0 | 136.1 | 136.1 | 136.1 | 117.8 | 117.8 |
| | $S_g$ | $m^2/g$ | 0.12 | 0.24 | 0.15 | 3.2 | 3.2 | 3.2 | 9.36 | 9.36 |
| | $k_s$ | mole/min/$m^2$ | 0.0026 | 0.0008 | 0.0010 | 0.0005 | 0.0003 | 0.0007 | 0.0003 | 0.0002 |
| | $k_p$ | $m^2$/mole | 21.3 | 108.1 | 57.4 | 634.6 | 575.5 | 567.8 | 1183.0 | 1163.9 |
| | $k_1$ | 1/min | 0.033 | 0.027 | 0.019 | 0.227 | 0.123 | 0.303 | 0.299 | 0.220 |
| | $k_2$ | – | 1.67 | 3.12 | 2.90 | 1.457 | 1.322 | 1.304 | 1.073 | 1.055 |
| | $k_s \cdot k_p$ | 1/min | 0.055 | 0.084 | 0.055 | 0.331 | 0.163 | 0.395 | 0.323 | 0.234 |
| | $r^2$ | – | 0.81 | 0.85 | 0.93 | 0.98 | 0.98 | 0.93 | 0.99 | 0.99 |

[a]Operated at an L/S = 10 mL $g^{-1}$, a partial pressure of $CO_2$ = 700 psig, 160 °C, and 12 h
[b]Operated for 120 min at 25 °C, $CO_2$ flow rate = 1 L/min, slurry volume = 350 mL, and L/S ratio = 20:1
[c]Operated at 65 °C and 750 rpm
[d]Operated at 65 °C and 1000 rpm

autoclave reactor and the slurry reactor. It suggests that the carbonation of steel slag should be integrated with co-utilizing alkaline wastewater (i.e., CRW) in the high-gravity carbonation process.

Similarly, the $k_p$ values for high-gravity carbonation is greater than that for slurry reactor and autoclave reactor, as follows:

- High-gravity carbonation process: 1164–1183 $m^2$/mol
- Slurry reactor: 567–634 $m^2$/mol
- Autoclave reactor: 21–108 $m^2$/mol

This indicates that the reaction product covers the surface of solid wastes more uniformly in the cases of the high-gravity carbonation and the slurry reactor, whereas the product builds up more cluster-like and covers less of the surface of steel slag in the autoclave reactor. In all cases, the fresh steelmaking slag possesses a smooth surface before carbonation but then exhibits characteristics such as rhombohedral, cubic, or needle-like $CaCO_3$ crystals on the surface of reacted slags after carbonation [44].

## 7.4 Mass Transfer Models

Since the accelerated carbonation has been regarded as a diffusion-controlled reaction (i.e., mass transfer limited) [5, 11, 15], mass transfer among phases is a key to effective carbonation for $CO_2$ capture. The mass transfer model for the carbonation process can be developed based on several classical models, e.g., two-film theory.

### *7.4.1 General Concepts and Key Parameters*

Mass transfer involves the movement of an element or molecular (mass) from one phase into another phase. It occurs in many processes; for example, dissolution of gaseous $CO_2$ in solution is the mass transfer phenomena. In classical, the mass transfer rate of a component mass can be described by two-film theory, where the rate of mass transfer is proportional to a mass transfer coefficient. The important mass transfer characteristics, especially for $CO_2$ absorption and/or dissolution, include overall gas-phase mass transfer coefficient ($K_G a$) and height of a transfer unit (HTU).

The solid–liquid mass transfer coefficient can be occasionally correlated as itself, where such correlations are specific to the system under consideration and are not generally applicable [52]. The Sherwood number ($Sh$) and the Colburn $J_d$ factor relate the physical properties of the system to the mass transfer coefficient and are more often used. To determine the gas-phase mass transfer coefficient in a

heterogeneous system (containing gas, liquid, and solid phases), several assumptions can be made:

- The effect of an inclined gas–liquid interface is neglected.
- The concentration of the liquid at the particle surface is equal to the saturation concentration of the solution (the mass transfer between the liquid and the solid is neglected).
- The changes in size and surface area of solid particles are neglected.
- The solid distribution throughout the bed is uniform.
- The Grashof ($Gr$) number is determined by the mean radius of the packed bed.

As described in the two-film theory, the $K_G a$ ($s^{-1}$) in a packed bed can be determined by Eq. (7.29):

$$\frac{1}{K_G a_e} = \frac{1}{k_G a_e} + \frac{H}{I(k_L a_e)} \tag{7.29}$$

where $k_G$ (m $s^{-1}$) is gas-side mass transfer coefficient; $a_e$ ($m^2$ $m^{-3}$) is effective surface area per unit volume of packed bed (gas–liquid interfacial); $I$ (–) is the enhancement factor; and $H$ is the Henry's law constant, expressed as the ratio of the partial pressure in the gas phase to the mass concentration in the liquid phase.

On the other hand, the relationship between mass transfer coefficient and diffusivity can be expressed as Eq. (7.30):

$$k_{CO_2} = \frac{D_{CO_2}}{\delta} \tag{7.30}$$

where $D_{CO_2}$ ($m^2$/s) is the diffusivity; $\delta$ is the film thickness (m); and $k_{CO_2}$ is the mass transfer coefficient (m/s). Table 7.3 presents several key thermodynamic state variables of $CO_2$ and water for model development. More thermodynamic state parameters for $CO_2$ and water can be also referred to Chap. 3.

The diffusivity of $CO_2$ in water ($m^2$/s) can be estimated by various methods, such as Eq. (7.31) [53] or Eq. (7.32) [54]:

$$D_{CO_2\_H_2O} = 2.35 \times 10^{-6} \times \exp(-2119/T) \tag{7.31}$$

$$D_{CO_2\_H_2O} = 1.81 \times 10^{-6} \times \exp(-16900/RT) \tag{7.32}$$

### 7.4.2 Incorporation with Reaction Kinetics

Direct carbonation is a heterogeneous reaction, i.e., containing the gas, liquid, and solid phases. It consists of mass transfer and chemical reaction. Therefore, a kinetic model can be developed for determining the reaction rate constant of carbonation ($k_c$) under different experimental conditions based on the shell mass balance.

**Table 7.3** Key thermodynamic state variables of $CO_2$ and water for mass transfer model development at 1 atm and 30 °C

| Abbreviation | Properties | Units | Values |
|---|---|---|---|
| $\rho_G$ | Density of gas ($CO_2$) | mole $cm^{-3}$ | $4.02 \times 10^{-5}$ |
| | | $kg/m^3$ | 1.778 |
| $\rho_L$ | Density of water | $kg/m^3$ | 995.7 |
| $\mu_G$ | Viscosity of gas ($CO_2$) | kg/m/s | $1.53 \times 10^{-5}$ |
| | | centipoise (cp) | $1.53 \times 10^{-2}$ |
| | | lb $s/ft^2$ | $3.19 \times 10^{-7}$ |
| $\mu_L$ | Dynamic viscosity of water | kg/m/s | $7.97 \times 10^{-4}$ |
| $\nu_G$ | Kinematic viscosity of gas | $m^2/s$ | $8.53 \times 10^{-6}$ |
| $\nu_L$ | Kinematic viscosity of liquid (water) | $m^2/s$ | $8.00 \times 10^{-7}$ |
| $D_{G\_air}$ | Diffusivity of $CO_2$ gas in air | $m^2/s$ | $1.60 \times 10^{-5}$ |
| $D_{G\_water}$ | Diffusivity of $CO_2$ gas in water | $m^2/s$ | $1.92 \times 10^{-9}$ |
| $\sigma_L$ | Surface tension of water | $kg/s^2$ | $7.12 \times 10^{-2}$ |
| $\sigma_c$ | Surface tension of packing[a] | $kg/s^2$ | $7.50 \times 10^{-2}$ |
| $H_{CO_2}$ | Henry's constant of $CO_2$ in water | mole/$cm^3$/atm | $2.98 \times 10^{-5}$ |

[a]For metal packing

The gas phase can be characterized by convection behaviors between the gas inlet and outlet, indicating that the mass transfer phenomenon of $CO_2$ between the gas and liquid was significant. In addition, the chemical reaction between total inorganic carbon (TIC) concentration in the liquid and the calcium species from the solid should be considered. The following assumptions could be made to simplify the mathematical model:

- The reaction remains at a temperature of 30 °C, where calcium carbonate ($CaCO_3$) is the major product.
- The mass transfer between the liquid and the solid is neglected.
- Total inorganic carbon concentration in liquid phase ($C_{TIC}$) is a constant.
- The carbonation conversion ($\delta_{Ca}$) in solid phase is a function of reaction time.

Thus, the apparent kinetic model of direct carbonation can be described by the mass balance over a thin shell of gas fluid with the reactor. The $CO_2$ concentration in exhaust gas ($C_{CO_2}$, dimensionless) is expressed in Eq. (7.33):

$$\rho_g V_g \frac{dC_{CO_2}}{dt} = \rho_g(Q_{g,i}C_{CO_2,i} - Q_{g,o}C_{CO_2}) - k_L a_p V_l(P_{CO_2}H_{CO_2} - C_{TIC}) \quad (7.33)$$

where $\rho_g$ (mole $cm^{-3}$) is the $CO_2$ gas density at the operating condition; $V_g$ ($cm^3$) and $V_l$ ($cm^3$) are the volumes of gas and liquid; $t$ (s) is the reaction time; $k_L$ (cm $s^{-1}$) is the liquid-phase mass transfer coefficient; $a_p$ ($cm^2$ $cm^{-3}$) is the specific surface area of packing materials; $H_{CO_2}$ (mole $cm^{-3}$ $atm^{-1}$) is the Henry's constant of $CO_2$ in water; and $C_{TIC}$ (mole $cm^{-3}$) is TIC concentration in the liquid phase. The consumption rate of TIC in the liquid phase can be expressed by Eq. (7.34):

$$V_l \frac{dC_{TIC}}{dt} = k_L a_p V_l (P_{CO_2} H_{CO_2} - C_{TIC}) + k_c C_{TIC} V_l (C_S - C_{S,0}) \tag{7.34}$$

where $k_c$ ($cm^3\ mol^{-1}\ s^{-1}$) is the rate constant of the carbonation reaction; and $C_s$ ($mol\ cm^{-3}$) is the CaO concentration of alkaline solid waste. It is assumed that the reaction was at steady state because the TIC concentration remained relatively unchanged during the carbonation. Therefore, Eq. (7.35) became:

$$k_L a_p V_l (C_{TIC} - P_{CO_2} H_{CO_2}) = k_c C_{TIC} V_l (C_S - C_{S,0}) \tag{7.35}$$

Substituting Eq. (7.35) into Eq. (7.33), the following kinetic equation can be obtained:

$$\rho_g V_g \frac{dC_{CO_2}}{dt} = \rho_g (Q_{g,i} C_{CO_2,i} - Q_{g,o} C_{CO_2,o}) + k_c C_{TIC} V (C_S - C_{S,0})_l \tag{7.36}$$

On the other hand, the rate of the solid concentration can be described by Eq. (7.37):

$$V_s \frac{dC_s}{dt} = k_c C_{TIC} C_s V_l \tag{7.37}$$

It was assumed that $C_s$ was a function of carbonation conversion and also substituted the liquid volume ($V_l$) by solid volume ($V_s$), as expressed in Eqs. (7.38) and (7.39), respectively.

$$C_s = C_{s0}(1 - \delta_{CaO}) \tag{7.38}$$

$$V_l = \rho_s V_s \frac{L}{S} \tag{7.39}$$

where $C_{s0}$ is the initial solid concentration ($mole\ cm^{-3}$). Thus, we can rearrange and integrate Eq. (7.37) by substituting Eqs. (7.38) and (7.39) into it:

$$\int \frac{d\delta_{CaO}}{1 - \delta_{CaO}} = \rho_s \frac{L}{S} k_c C_{TIC} \int dt \tag{7.40}$$

or

$$\delta_{CaO} = 1 - \exp^{\left(-\rho_s \frac{L}{S} k_c C_{TIC} t\right)} \tag{7.41}$$

As a result, the developed kinetic model could be validated by fitting Eq. (7.41) with the experimental data. Meanwhile, the reaction rate constant ($k_c$) can be estimated accordingly. According to the results in the literature [55], the rate constant for reaction using wastewater (i.e., cold-rolling wastewater (CRW)) with a slag particle size of less than 125 μm was the highest (216.9 $cm^3\ mol^{-1}\ s^{-1}$). In addition, the

carbonation reaction in the high-gravity carbonation should be accelerated by using wastewater (with a rate constant of 188–217 $cm^3\ mol^{-1}\ s^{-1}$) instead of DI water (with a rate constant of 160–195 $cm^3\ mol^{-1}\ s^{-1}$).

In addition, the liquid-phase mass transfer coefficient ($k_L$) can be determined using Eq. (7.42) by substituting Eq. (7.41) into Eq. (7.35).

$$k_c C_{TIC} C_{s0}\left(1-\exp^{\left(-\rho_s \frac{L}{S} k_c C_{TIC} t\right)}\right) = k_L a_p (P_{CO_2} H_{CO_2} - C_{TIC}) \tag{7.42}$$

The experimental results of carbonation could be well predicted by the developed kinetic model. For example, the mass transfer coefficient ($k_L a$) for reaction using wastewater with a slag particle size of less than 125 μm was the highest (i.e., $9.23\times10^{-4}\ s^{-1}$) [55].

## 7.4.3 Modelling for Various Types of Reactors

### 7.4.3.1 Slurry Bubble Column (SBC)

Slurry bubble column (SBC) mass transfer correlations are often derived from boundary layer theory where the Kolmogroff's isotropic turbulence theory has been applied [52]. The general correlations can be a variation of

$$Sh = 2 + bSc^m [e d_p^4 / v^3]^n \tag{7.43}$$

where $e$ is the energy dissipation term and defined as $U_g g$. The term of $m$ is often set equal to 1/3 as predicted by boundary layer theory.

Research has conducted different kinetic models to determine the rate-limiting step of mineral carbonation in a conventional bubble column [11, 22]. In fact, liquid–solid mass transfer is important and considered as the rate limiting factor in many cases of mineral carbonation [52, 56]. This might be due to the fact that minerals in solid matrix dissolve partly, and the passive layers are gradually formed, which increase resistance to mass transfer, and eventually lead to incomplete conversion.

### 7.4.3.2 Rotating Packed Bed (RPB)

Rotating packed bed (RPB) has been intensively applied and studied in many fields including gas absorption [57–59], stripping [60, 61], distillation [62], ozonation [63], deaeration [61], and biofuel production [64]. An RPB reactor has been introduced to improve the mass transfer rate among phases due to its high centrifugal forces and great micro-mixing ability. It thus can enhance mass transfer

between gas and liquid, and even between liquid and solid. The features of utilizing the RPB reactor for process intensification include [1, 58, 62, 65, 66] the following:

- It can provide a mean acceleration of hundreds, and even thousands, of times greater than the force of gravity.
- It can effectively lead to the formation of thin liquid films and micro- or nano-droplets.
- The overall mass transfer coefficient in an RPB, especially the liquid-side mass transfer coefficient, was greater than that in a packed column.
- The volumetric gas–liquid mass transfer coefficients are an order of magnitude higher than those in a conventional packed bed.
- Dramatic reductions in equipment size over that required for equivalent mass transfer in a gravity-flow-packed bed.
- If the tangential gas velocity in the rotor is nearly the same as that in the packing zone, the gas-side mass transfer coefficient is believed to be in the same range as that of the conventional packed columns.

1. Assumptions

Performance of the carbonation reaction using an RPB reactor (so-called high-gravity carbonation) was found to be better than using an autoclave or slurry reactor [10, 16, 67]. Over the past years, several theoretical models have been developed for describing mass transfer phenomena of RPB for gas–liquid absorption [56, 68]. However, a few studies on gas–liquid–solid mass transfer for the high-gravity carbonation of alkaline solid wastes have appeared in the literature. This is attributed to the fact that sophisticated assumptions and complicated, partial differential equation programming are usually required to determine the gas–liquid–solid mass transfer.

The solid–liquid mass transfer coefficient is occasionally correlated as itself; however, such correlations are specific to the system under consideration and are not generally applicable [52]. Precipitation is usually a rapid reaction and the mixing (especially micro-mixing) of the process is very important for particle size distribution [69]. Therefore, in high-gravity carbonation process, the carbonation reaction would be controlled by the intrinsic reaction kinetics due to the excellent micro-mixing and the fine particle size (with a particle size of 44–88 μm) [16, 55, 67]. Before the passive layers around particles are formed, the minerals in solid particle can be rapidly dissolved into solution when the solid particle is moved through the packed bed. This indicates that the mass transfer between liquid and solid phases may not be the rate-limiting factor in the high-gravity carbonation system.

2. Gas-phase mass transfer coefficient

The driving force between the saturated $CO_2$ concentration in the bulk gas and the $CO_2$ concentration on the surface of liquid film can be determined by mass balance over a thin shell of fluid with the RPB, as shown in Eq. (7.44):

$$\frac{1}{\rho_{CO_2}}\frac{dM_G}{dV} = K_G a_e (C_G^* - C_G^{'}) \tag{7.44}$$

where $dV$ can be expressed by Eq. (7.45):

$$dV = 2\pi r h \cdot dr \tag{7.45}$$

By substitution of Eq. (7.45) into Eq. (7.44), the overall gas-phase mass transfer coefficient ($K_G a$, $s^{-1}$) can be obtained as Eq. (7.46):

$$K_G a_e = \frac{M_G}{\rho_G h\pi(r_o^2 - r_i^2)}(NTU_G) = \frac{Q_G}{h\pi(r_o^2 - r_i^2)}\ln\left(\frac{C_{G,i}}{C_{G,o}}\right) \tag{7.46}$$

where $C_{G,i}$ (%) and $C_{G,o}$ (%) are $CO_2$ contents in inlet and outlet gas streams, respectively. The terms of $r_o$ (m) and $r_i$ (m) are the outside and inside radii of packed bed, respectively. In general, the $K_G a$ value increases with the gas flow rate, with the liquid flow rate, and mainly with the rotor speed [70]. Also since the $K_G a$ values in an RPB are an order of magnitude higher than those in a conventional packed bed, the reactor size of RPB could be much smaller than that of a conventional reactor such as slurry reactor and bubble column [58, 62].

Beside the $K_G a$ value, the height of transfer unit (HTU) and the area of transfer unit (ATU) are important mass transfer characteristics. The values of HTU and ATU can be calculated using Eqs. (7.47) and (7.48), respectively [71, 72]:

$$HTU = \frac{r_o - r_i}{NTU} = \frac{r_o - r_i}{\ln(C_{G,i}/C_{G,o})} \tag{7.47}$$

$$ATU = \frac{\pi(r_o^2 - r_i^2)}{NTU} = \frac{\pi(r_o^2 - r_i^2)}{\ln(C_{G,i}/C_{G,o})} \tag{7.48}$$

3. Liquid-phase mass transfer coefficient

In spite of the significant differences between RPB and traditional packed bed column, penetration theory can be capable of describing the liquid-side mass transfer behavior fairly well in RPB [73]. These correlations are most often expressed in terms of dimensionless numbers in the form of a power series. As described in the penetration theory, the liquid-side mass transfer coefficient ($k_L$) can be expressed in Eq. (7.49):

$$k_L = a\left(\frac{D_L}{d_p}\right) Sc_L^b Re_L^c Gr_L^d \tag{7.49}$$

where the terms of $a$, $b$, $c$, and $d$ are constants. The Grashof number, representing the ratio of gravitational to viscous forces, can be determined by Eq. (7.50):

$$Gr_L = g d_p^3 \left(\frac{\rho_L}{\mu_L}\right)^2 \tag{7.50}$$

In Eq. (7.50), the $g$ value (m/s$^2$) can be replaced by the centrifugal acceleration in the RPB, which can be determined by Eq. (7.51):

$$g = a_m = \left(\frac{r_o^2 + r_i^2}{2}\right)^{1/2} \omega^2 \tag{7.51}$$

where $\omega$ is the rotational speed (rad s$^{-1}$) at the mean radius of packed bed.

4. Empirical mass transfer models

In a conventional packed bed column, the commonly used model for liquid-side ($k_L$) and gas-side ($k_G$) mass transfer coefficient is originally developed by Onda et al. [74], as shown in Eqs. (7.52) and (7.53), respectively. It was suggested that the constant of 5.23 in Eq. (7.53) should be well correlated by changing the constant into 2.00 for smaller packings (when the diameter of packings is less than 1.5 cm).

$$k_L = 0.0051 \left(\frac{a_t}{a_w}\right)^{2/3} Re_L^{2/3} Sc_L^{-1/2} \left(\frac{\rho_L}{\mu_L g}\right)^{-1/3} (a_p d_p)^{0.4} \tag{7.52}$$

and

$$k_G = 5.23 (a_p D_G) Re_G^{0.7} Sc_G^{1/3} (a_p d_p)^{-2} \tag{7.53}$$

It is difficult to determine mass transfer coefficients separated from volumetric mass transfer coefficients $k_L a_e$ and $k_G a_e$, since the effective interfacial area ($a_e$) between the liquid phase and vapor phase is usually not known [62]. Several correlations could be used to estimate the wetted surface area ($a_w$), as shown in Eq. (7.54) [73, 75]. It suggests that the $a_w/a_t$ predicted value should be reliable under high-gravity RPB process, if packing materials with small static hold up (i.e., large packing size) the wetted area ($a_w$) may equal the interfacial area ($a_e$).

$$\frac{a_w}{a_t} = \frac{a_e}{a_t} = 1 - \exp\left[-1.45 \left(\frac{\sigma_c}{\sigma_L}\right)^{0.75} Re_L^{0.1} We_L^{0.2} Fr_L^{-0.05}\right] \tag{7.54}$$

Pan et al. [76] developed a correlation for $K_G a$ in the high-gravity carbonation process. In this model, the important operating parameters for high-gravity carbonation include gas flow rate, slurry flow rate, liquid-to-solid ratio, and rotation speed. The relevant models were obtained by the nonlinear regression of experimental data for estimation of both the $K_G a$ and HTU values:

$$K_G a_e = 0.01\left(\frac{a_t D_G}{d_p}\right) Re_G^{-1.16} Gr_G^{0.33} Re_L^{2.12} \tag{7.55}$$

$$\mathrm{HTU} = 0.0003\left(\frac{a_t D_G}{d_p}\right) Re_G^{2.16} Gr_G^{-0.33} Re_L^{-2.12} \tag{7.56}$$

where the ranges of the dimensionless groups in this correlation are as follows:

$$7.8 < Re_G < 15.9 \tag{7.57}$$

$$1.3 < Re_L < 2.2 \tag{7.58}$$

$$2.3 < Gr_G < 26.8 \tag{7.59}$$

Both the $K_G a$ and HTU values varied with the centrifugal acceleration to the 0.33 power. The dependence of liquid velocity on $K_G a$ value was much higher than that of gas velocity, indicating that the high-gravity carbonation of steel slag could exhibit a mass transfer resistance lay on the liquid side [76]. Figure 7.5 shows the comparison of the estimated $K_G a$ value by the models with the experimental data. The result indicates that the $K_G a$ values predicted by the developed model were similar to the experimental value, where the experimental $K_G a$ values lay within ±20% of the values estimated by Eq. (7.55).

In contrast, the effect of gas velocity on the HTU value was similar to that of liquid velocity. The overall mass transfer coefficient in high-gravity carbonation, especially the liquid-side mass transfer coefficient ($k_L a$), was greater than in packed bed columns [76]. It is noted that since the tangential gas velocity in the rotor is

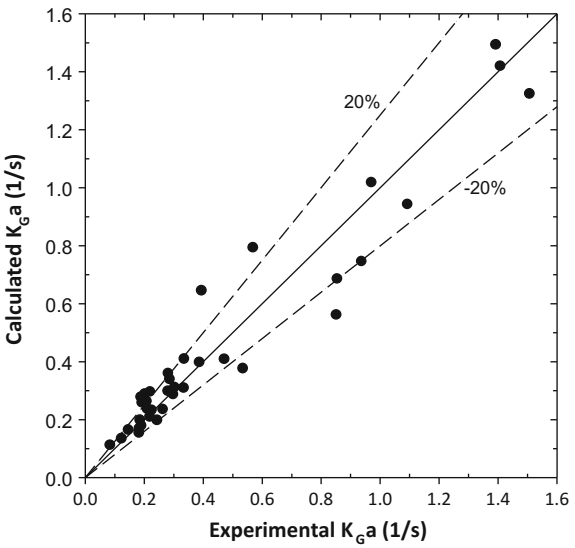


**Fig. 7.5** Comparison of experimental and calculated $K_G a$ values for high-gravity carbonation process model. Reprinted by permission from Macmillan Publishers Ltd: Ref. [76], copyright 2015

nearly the same as that in the packing zone, the gas-side mass transfer coefficient should be in the same range as that of the conventional packed column [66]. The results in the literature indicate [55] that the $k_L a$ value for high-gravity reaction with a steel slag particle size of less than 125 μm was $9.23 \times 10^{-4}$ $s^{-1}$, based on the shell mass balance model.

## References


1. Wang M (2004) Controlling factors and mechanism of preparing needlelike $CaCO_3$ under high-gravity environment. Powder Technol 142(2–3):166–174. doi:10.1016/j.powtec.2004.05.003
2. Thiery M, Villain G, Dangla P, Platret G (2007) Investigation of the carbonation front shape on cementitious materials: effects of the chemical kinetics. Cem Concr Res 37(7):1047–1058. doi:10.1016/j.cemconres.2007.04.002
3. Montes-Hernandez G, Perez-Lopez R, Renard F, Nieto JM, Charlet L (2009) Mineral sequestration of $CO_2$ by aqueous carbonation of coal combustion fly-ash. J Hazard Mater 161 (2–3):1347–1354. doi:10.1016/j.jhazmat.2008.04.104
4. Tsuyoshi S, Etsuo S, Minoru M, Nobuaki O (2010) Carbonation of γ-$Ca_2SiO_4$ and the mechanism of vaterite formation. J Adv Concr Technol 8(3):273–280
5. Pan S-Y, Chang EE, Chiang P-C (2012) $CO_2$ capture by accelerated carbonation of alkaline wastes: a review on its principles and applications. Aerosol Air Qual Res 12:770–791. doi:10.4209/aaqr.2012.06.0149
6. Fernandez Bertos M, Simons SJ, Hills CD, Carey PJ (2004) A review of accelerated carbonation technology in the treatment of cement-based materials and sequestration of $CO_2$. J Hazard Mater 112(3):193–205. doi:10.1016/j.jhazmat.2004.04.019
7. Huntzinger DN, Gierke JS, Kawatra SK, Eisele TC, Sutter LL (2009) Carbon dioxide sequestration in cement kiln dust through mineral carbonation. Environ Sci Technol 43 (6):1986–1992
8. Uibu M, Kuusik R (2009) Mineral trapping of $CO_2$ via oil shale ash aqueous carbonation: controlling mechanism of process rate and development of continuous-flow reactor system. Oil Shale 26(1):40. doi:10.3176/oil.2009.1.06
9. Huijgen WJJ, Ruijg GJ, Comans RNJ, Witkamp GJ (2006) Energy consumption and net $CO_2$ sequestration of aqueous mineral carbonation. Ind Eng Chem Res 45(26):9184–9194
10. Pan SY, Chiang PC, Chen YH, Chen CD, Lin HY, Chang EE (2013) Systematic approach to determination of maximum achievable capture capacity via leaching and carbonation processes for alkaline steelmaking wastes in a rotating packed bed. Environ Sci Technol 47 (23):13677–13685. doi:10.1021/es403323x
11. Lekakh SN, Rawlins CH, Robertson DGC, Richards VL, Peaslee KD (2008) Kinetics of aqueous leaching and carbonization of steelmaking slag. Metall Mat Trans B 39(1):125–134. doi:10.1007/s11663-007-9112-8
12. Costa G (2009) Accelerated carbonation of minerals and industrial residues for carbon dioxide storage. Università delgi Studi di Roma
13. Eloneva S, Said A, Fogelholm C-J, Zevenhoven R (2012) Preliminary assessment of a method utilizing carbon dioxide and steelmaking slags to produce precipitated calcium carbonate. Appl Energy 90(1):329–334. doi:10.1016/j.apenergy.2011.05.045
14. Kodama S, Nishimoto T, Yamamoto N, Yogo K, Yamada K (2008) Development of a new pH-swing $CO_2$ mineralization process with a recyclable reaction solution. Energy 33(5):776–784. doi:10.1016/j.energy.2008.01.005

15. Chang EE, Wang Y-C, Pan S-Y, Chen Y-H, Chiang P-C (2012) $CO_2$ capture by using blended hydraulic slag cement via a slurry reactor. Aerosol Air Qual Res 12:1433–1443. doi:10.4209/aaqr.2012.08.0210
16. Chang EE, Pan SY, Chen YH, Tan CS, Chiang PC (2012) Accelerated carbonation of steelmaking slags in a high-gravity rotating packed bed. J Hazard Mater 227–228:97–106. doi:10.1016/j.jhazmat.2012.05.021
17. Pan SY, Liu HL, Chang EE, Kim H, Chen YH, Chiang PC (2016) Multiple model approach to evaluation of accelerated carbonation for steelmaking slag in a slurry reactor. Chemosphere 154:63–71. doi:10.1016/j.chemosphere.2016.03.093
18. Zumdahl SS (2009) Chemical principles, 6th edn. Houghton Mifflin Company
19. Li X, Bertos MF, Hills CD, Carey PJ, Simon S (2007) Accelerated carbonation of municipal solid waste incineration fly ashes. Waste Manag 27(9):1200–1206. doi:10.1016/j.wasman.2006.06.011
20. Fernandez Bertos M, Li X, Simons SJR, Hills CD, Carey PJ (2004) Investigation of accelerated carbonation for the stabilisation of MSW incinerator ashes and the sequestration of $CO_2$. Green Chem 6(8):428. doi:10.1039/b401872a
21. Chang EE, Pan S-Y, Chen Y-H, Chu H-W, Wang C-F, Chiang P-C (2011) $CO_2$ sequestration by carbonation of steelmaking slags in an autoclave reactor. J Hazard Mater 195:107–114. doi:10.1016/j.jhazmat.2011.08.006
22. Chang EE, Chen CH, Chen YH, Pan SY, Chiang PC (2011) Performance evaluation for carbonation of steel-making slags in a slurry reactor. J Hazard Mater 186(1):558–564. doi:10.1016/j.jhazmat.2010.11.038
23. Ishida T, Maekawa K (2000) Modeling of pH profile in pore water based on mass transport and chemical equilibrium theory. In: Proceedings of JSCE, 2000
24. Druckenmiller ML, Maroto-Valer MM (2005) Carbon sequestration using brine of adjusted pH to form mineral carbonates. Fuel Process Technol 86(14–15):1599–1614. doi:10.1016/j.fuproc.2005.01.007
25. Tai CY, Chen WR, Shih S-M (2006) Factors affecting wollastonite carbonation under $CO_2$ supercritical conditions. AIChE J 52(1):292–299. doi:10.1002/aic.10572
26. Park A, Fan L (2004) Mineral sequestration: physically activated dissolution of serpentine and pH swing process. Chem Eng Sci 59(22–23):5241–5247. doi:10.1016/j.ces.2004.09.008
27. Dijkstra JJ, Meeussen JCL, Comans RNJ (2004) Leaching of heavy metals from contaminated soils: an experimental and modeling study. Environ Sci Technol 38(16):4390–4395. doi:10.1021/es049885v
28. De Windt L, Chaurand P, Rose J (2011) Kinetics of steel slag leaching: batch tests and modeling. Waste Manag 31(2):225–235. doi:10.1016/j.wasman.2010.05.018
29. Iizuka A, Fujii M, Yamasaki A, Yanagisawa Y (2004) Development of a new $CO_2$ sequestration process utilizing the carbonation of waste cement. Ind Eng Chem Res 43(24):7880–7887. doi:10.1021/ie0496176
30. Alexander G, Maroto-Valer MM, Aksoy P, Schobert H (2005) Development of a $CO_2$ sequestration module by integrating mineral activation and aqueous carbonation. The Pennsylvania State University
31. Park AHA, Jadhav R, Fan LS (2003) $CO_2$ mineral sequestration: chemically enhanced aqueous carbonation of serpentine. Can J Chem Eng 81(3–4):885–890
32. O'Connor WK, Dahlin DC, Rush GE, Dahlin CL, Collins WK (2002) Carbon dioxide sequestration by direct mineral carbonation: process mineralogy of feed and products. Miner Metall Proc 19(2):95–101
33. Santos A, Ajbary M, Morales-Florez V, Kherbeche A, Pinero M, Esquivias L (2009) Larnite powders and larnite/silica aerogel composites as effective agents for $CO_2$ sequestration by carbonation. J Hazard Mater 168(2–3):1397–1403. doi:10.1016/j.jhazmat.2009.03.026
34. Morel FMM, Hering JG (1993) Principles and applications of aquatic chemistry. Wiley
35. Edsall JT, Wyman J (1958) Biophysical chemistry. Academic Press
36. Stumm W, Morgan JJ (1996) Aquatic chemistry. A Wiley-Interscience Publication, Wiley

37. Lagasa AC (1995) Fundamental approaches to describing mineral dissolution and precipitation rates. In: White AF, Brantley SL (eds) Reviews in mineralogy, vol 31. Mineralogical Society of America, Washington, D.C., pp 23–86
38. Gerdemann SJ, O'Connor WK, Dahlin DC, Penner LR, Rush H (2007) Ex situ aqueous mineral carbonation. Environ Sci Technol 41(7):2587–2593
39. Huijgen WJJ, Comans RNJ (2006) Carbonation of steel slag for $CO_2$ sequestration: leaching of products and reaction mechanisms. Environ Sci Technol 40(8):2790–2796
40. Alexander G, Mercedesmarotovaler M, Gafarovaaksoy P (2007) Evaluation of reaction variables in the dissolution of serpentine for mineral carbonation. Fuel 86(1–2):273–281. doi:10.1016/j.fuel.2006.04.034
41. Krevor SCM, Lackner KS (2011) Enhancing serpentine dissolution kinetics for mineral carbon dioxide sequestration. Int J Greenhouse Gas Control 5(4):1073–1080. doi:10.1016/j.ijggc.2011.01.006
42. Bhatia SK, Perlmutter DD (1983) Effect of the product layer on the kinetics of the $CO_2$-lime reaction. AIChE J 29(1):79–86
43. Liu W, Dennis JS, Sultan DS, Redfern SAT, Scott SA (2012) An investigation of the kinetics of $CO_2$ uptake by a synthetic calcium based sorbent. Chem Eng Sci 69:644–658
44. Pan S-Y, Chiang P-C, Chen Y-H, Tan C-S, Chang EE (2014) Kinetics of carbonation reaction of basic oxygen furnace slags in a rotating packed bed using the surface coverage model: maximization of carbonation conversion. Appl Energy 113:267–276. doi:10.1016/j.apenergy.2013.07.035
45. Sohn HY, Szekely J (1973) Reactions between solids through gaseous intermediates—I reactions controlled by chemical kinetics. Chem Eng Sci 28:1789–1801
46. Chang EE, Chiu A-C, Pan S-Y, Chen Y-H, Tan C-S, Chiang P-C (2013) Carbonation of basic oxygen furnace slag with metalworking wastewater in a slurry reactor. Int J Greenhouse Gas Control 12:382–389. doi:10.1016/j.ijggc.2012.11.026
47. Li X, Yang Z, Zhao J, Wang Y, Song R, He Y, Su Z, Lei T (2015) A modified shrinking core model for the reaction between acid and hetero-granular rough mineral particles. Hydrometallurgy 153:114–120. doi:10.1016/j.hydromet.2015.03.001
48. Sohn HY (2004) The effects of reactant starvation and mass transfer in the rate measurement of fluid–solid reactions with small equilibrium constants. Chem Eng Sci 59(20):4361–4368. doi:10.1016/j.ces.2004.06.033
49. Daval D, Martinez I, Corvisier J, Findling N, Goffé B, Guyot F (2009) Carbonation of Ca-bearing silicates, the case of wollastonite: experimental investigations and kinetic modeling. Chem Geol 265(1–2):63–78. doi:10.1016/j.chemgeo.2009.01.022
50. Chang EE, Pan SY, Yang L, Chen YH, Kim H, Chiang PC (2015) Accelerated carbonation using municipal solid waste incinerator bottom ash and cold-rolling wastewater: performance evaluation and reaction kinetics. Waste Manag 43:283–292. doi:10.1016/j.wasman.2015.05.001
51. Shih SM, Ho CS, Song YS, Lin JP (1999) Kinetics of the reaction of Ca(OH)(2) with $CO_2$ at low temperature. Ind Eng Chem Res 38(4):1316–1322
52. Arters DC, Fan L-S (1986) Experimental methods and correlation of solid liquid mass transfer in fluidized beds. Chem Eng Sci 41(1):107–115
53. Versteeg GF, Swaalj WV (1988) Solubility and diffusivity of acid gases (carbon dioxide, nitrous oxide) in aqueous alkanolamine solutions. J Chem Eng Data 33(1):29–34
54. Frank MJW, Kuipers JAM, van Swaaij WPM (1996) Diffusion coefficients and viscosities of $CO_2$ + $H_2O$, $CO_2$ + $CH_3OH$, NH3 + $H_2O$ and $NH_3$ + $CH_3OH$ liquid mixtures. J Chem Eng Data 41:297–302
55. Chang EE, Chen T-L, Pan S-Y, Chen Y-H, Chiang P-C (2013) Kinetic modeling on $CO_2$ capture using basic oxygen furnace slag coupled with cold-rolling wastewater in a rotating packed bed. J Hazard Mater 260:937–946. doi:10.1016/j.jhazmat.2013.06.052
56. Munjal S, Dudukovic MP, Ramachandran P (1989) Mass-transfer in rotating packed beds—I. Dev Gas-Liquid Liquid-Solid Mass Transf Correl Chem Eng Sci 44(10):2245–2256

57. Cheng H-H, Tan C-S (2011) Removal of $CO_2$ from indoor air by alkanolamine in a rotating packed bed. Sep Purif Technol 82:156–166. doi:10.1016/j.seppur.2011.09.004
58. Tan C, Chen J (2006) Absorption of carbon dioxide with piperazine and its mixtures in a rotating packed bed. Sep Purif Technol 49(2):174–180. doi:10.1016/j.seppur.2005.10.001
59. Lin CC, Lin YH, Tan CS (2010) Evaluation of alkanolamine solutions for carbon dioxide removal in cross-flow rotating packed beds. J Hazard Mater 175(1–3):344–351. doi:10.1016/j.jhazmat.2009.10.009
60. Guo F, Zheng C, Guo K, Feng YD, Gardner NC (1997) Hydrodynamics and mass transfer in crossflow rotating packed bed. Chem Eng Sci 52(21–22):3853–3859
61. Chen YS, Lin FY, Lin CC, Tai CYD, Liu HS (2006) Packing characteristics for mass transfer in a rotating packed bed. Ind Eng Chem Res 45(20):6846–6853
62. Kelleher T, Fair JR (1996) Distillation studies in a high-gravity contactor. Ind Eng Chem Res 35:4646–4655
63. Chen YH, Chang CY, Su WL, Chen CC, Chiu CY, Yu YH, Chiang PC, Chiang SIM (2004) Modeling ozone contacting process in a rotating packed bed. Ind Eng Chem Res 43(1):228–236
64. Chen YH, Huang YH, Lin RH, Shang NC (2010) A continuous-flow biodiesel production process using a rotating packed bed. Bioresour Technol 101(2):668–673. doi:10.1016/j.biortech.2009.08.081
65. Lin C, Chen B (2008) Characteristics of cross-flow rotating packed beds. J Ind Eng Chem 14(3):322–327. doi:10.1016/j.jiec.2008.01.004
66. Chandra A, Goswami PS, Rao DP (2005) Characteristics of flow in a rotating packed bed (HIGEE) with split packing. Ind Eng Chem Res 44(11):4051–4060
67. Pan SY, Chiang PC, Chen YH, Tan CS, Chang EE (2013) Ex situ $CO_2$ capture by carbonation of steelmaking slag coupled with metalworking wastewater in a rotating packed bed. Environ Sci Technol 47(7):3308–3315. doi:10.1021/es304975y
68. Zhao B, Su Y, Tao W (2014) Mass transfer performance of $CO_2$ capture in rotating packed bed: dimensionless modeling and intelligent prediction. Appl Energy 136:132–142. doi:10.1016/j.apenergy.2014.08.108
69. Xiang Y, Wen LX, Chu GW, Shao L, Xiao GT, Chen JF (2010) Modeling of the precipitation process in a rotating packed bed and its experimental validation. Chin J Chem Eng 18(2):249–257
70. Liu H, Kuo C (1996) Quantitative multiphase determination using the Rietveld method with high accuracy. Mater Lett 26:171–175
71. Sandilya P, Rao DP, Sharma A (2001) Gas-phase mass transfer in a centrifugal contactor. Ind Eng Chem Res 40:384–392
72. Cheng H-H, Shen J-F, Tan C-S (2010) $CO_2$ capture from hot stove gas in steel making process. Int J greenhouse gas control 4(3):525–531. doi:10.1016/j.ijggc.2009.12.006
73. Tung HH, Mah RSH (1985) Modeling liquid mass transfer in HIGEE separation process. Chem Eng Commun 39:147–153
74. Onda K, Takeuchi H, Okumoto Y (1968) Mass transfer coefficients between gas and liquid phases in packed columns. J Chem Eng Jpn 1(1):56–62
75. Perry RH, Chilton CH (1973) Chemical engineers' handbook. McGraw-Hill, New York. doi:10.1002/aic.690200140
76. Pan SY, Eleazar EG, Chang EE, Lin YP, Kim H, Chiang PC (2015) Systematic approach to determination of optimum gas-phase mass transfer rate for high-gravity carbonation process of steelmaking slags in a rotating packed bed. Appl Energy 148:23–31. doi:10.1016/j.apenergy.2015.03.047